1

"Classical" Gaseous Detectors and Their Limits

Resistive gaseous detectors are a family of detectors of charged particles, energetic photons, and neutrons, whose active medium is a gas, and which are characterized by having at least one of the electrodes made of resistive materials, whose resistivity typically ranges in the 10^8–10^{12} Ω cm interval. The main advantage of these devices is that they are intrinsically spark protected, even if at the price of being counting rate limited. To appreciate in practice the importance of this feature, it will be useful to briefly review some main designs of traditional gaseous detectors that existed before the implementation of resistive electrodes, and the principles they operate upon.

1.1 Ionization Chambers

Historically, the first gaseous detector used in experimental measurements at the beginning of the last century was the so-called ionization chamber. This detector, depending on the experimental requirements, can have different geometries: planar, cylindrical, spherical, and so on. However, its principle of operation is independent of its geometry.

The drawings of a planar and a cylindrical ionization chamber are shown schematically in Figure 1.1. Ionization chambers consist of two metallic electrodes: anode and cathode, between which an adequate voltage difference is applied. Such detectors can operate filled with various gases (including air), typically at a pressure around 1 atm. They are still used today, even outside the field of high-energy physics, for instance, in smoke detectors, and in particular mostly for dosimetry applications (see Wikipedia, The Free Encyclopedia, 2017 and references therein, and Chapter 6 of Khan and Gibbon, 2014).

If an intense flux of ionizing radiation (either X-rays, or γ-rays or charged particles, which produce in the gas a certain number of ion-electron pairs) impinges in the region between the electrodes, the resulting current, measured as a function of the applied voltage, will look as schematically shown in Figure 1.2. At low voltages (roughly below 1 kV, depending on the specific geometry and gas used), it will grow until reaching a kind of saturation region – usually called

Resistive Gaseous Detectors: Designs, Performance, and Perspectives, First Edition.
Marcello Abbrescia, Vladimir Peskov, and Paulo Fonte.

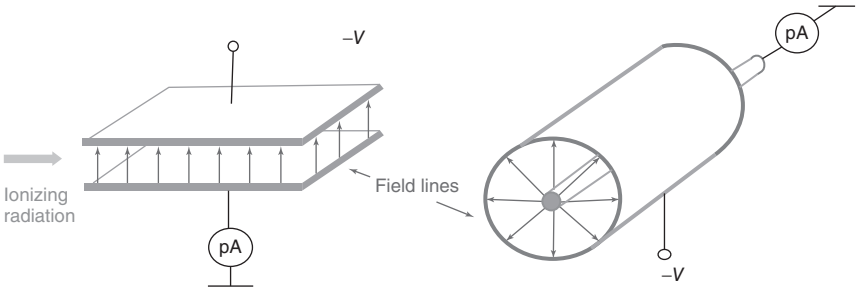

Figure 1.1 Schematic drawings of a planar and a cylindrical ionization chamber; "pA" stands pico-Amperometers, i.e. devices used to measure very small amounts of current.

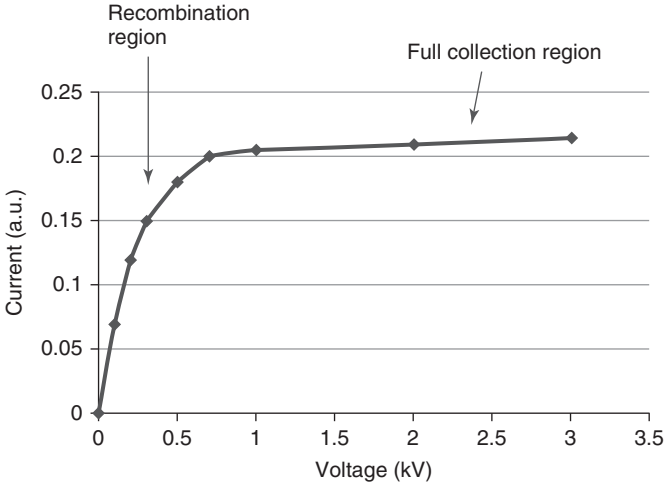

Figure 1.2 Typical current versus applied voltage curve, measured with an ionization chamber, when irradiated by a flux of photons or charged particles.

a "plateau." In this region, practically all primary electron-ion pairs produced by the impinging ionizing radiation are collected on the electrodes. At voltages below the plateau region, some electron-ion pairs recombine, and this is the reason why the collected current is lower than the saturated value.

The value of the current in the plateau region is given by

$$I = k_i \frac{W_{\text{dep}}}{W_{\text{i}}}, \tag{1.1}$$

where k_{i} is a coefficient W_{dep} is the energy deposited by the ionizing radiation inside the volume of the ionization chamber and W_{i} is the mean energy required for the creation of a single electron-ion pair. Note that W_{i} is higher than the ionization potential (typically twice more) because part of the energy deposited by the ionizing particles goes in other energy dissipating channels (excitation of atomic energy levels or excitation of molecular electronic, vibrational and rotational degrees of freedom, for instance) which do not produce ion/electron pairs in the gas.

In the case of X-rays, for instance:

$$W_{\text{dep}} = \int N_{\text{abs}}(\nu) E_{\text{v}} \mathrm{d}\nu \tag{1.2}$$

where $N_{\text{abs}}(\nu)$ is the number of photons with energy E_{v} absorbed in the detector unit volume and ν the frequency of the impinging radiation.

The capability of ionization chambers to detect radiation is determined by the sensitivity of the current meter used to measure the current flowing between the two electrodes; since this, at the beginning of the last century, was relatively low compared to the present standards, this kind of detectors could detect only relatively high intensity radiation, and not single photons or ionizing particles.

1.2 Single-Wire Counters Operated in Avalanche Mode

The first gaseous detector able to record individual photons and elementary particles was the avalanche counter, invented by Rutherford and Geiger (1908). This detector is schematically shown in Figure 1.3. It is a metallic cylinder (with a typical diameter of 2–3 cm) in the center of which a thin metallic wire with diameter

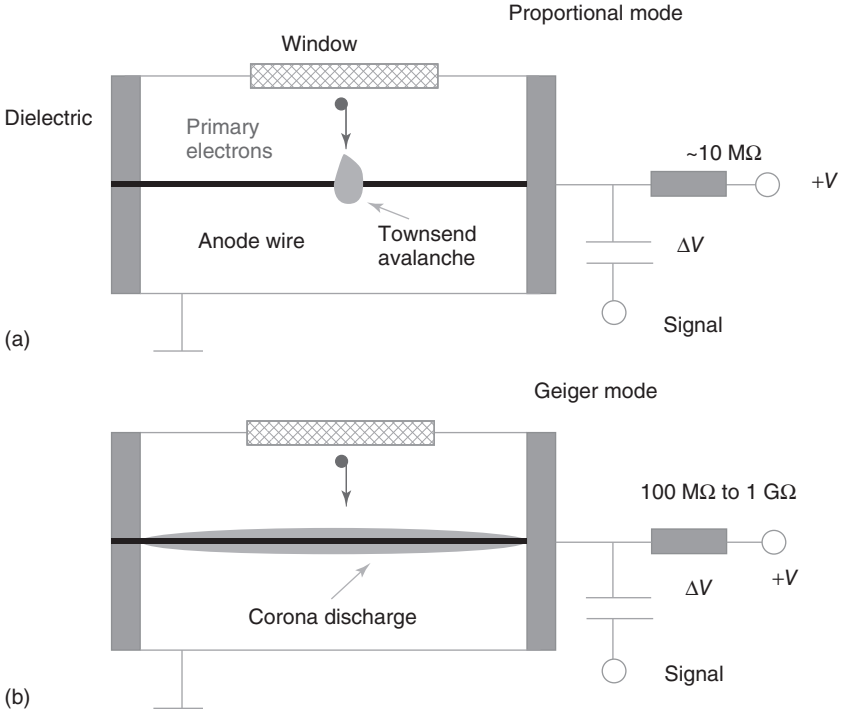

Figure 1.3 Schematic drawings of a single-wire cylindrical counter invented by Geiger and Rutherford in 1908. This detector is usually exploited either in a proportional mode (a) or in a so-called Geiger mode (b).

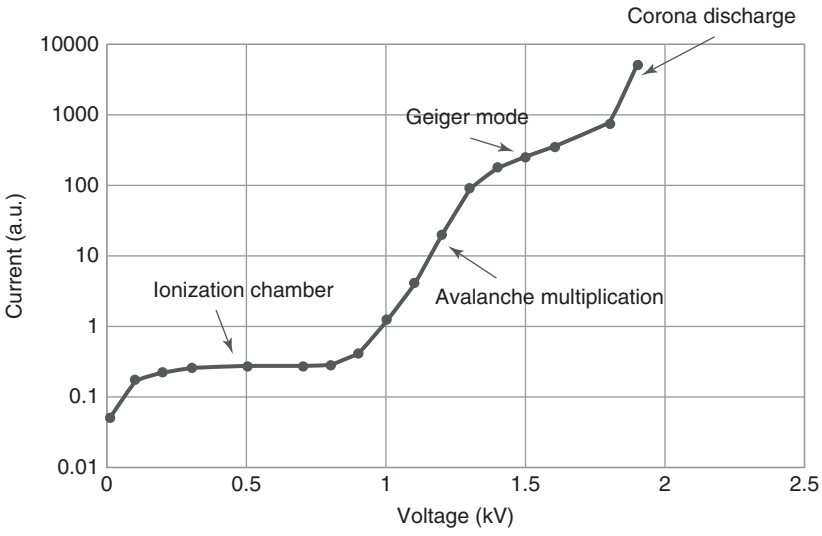

Figure 1.4 Typical voltage–current characteristics for a single-wire counter irradiated by photons or charged particles.

around 0.1 mm or below is stretched. A positive voltage is applied to the central wire while the cylinder is connected to the ground.

The typical voltage–current characteristic curve of this detector, when subject to an intense radiation source, is shown in Figure 1.4. Just like for the previous figure, the values of the voltages and currents are to be intended as order of magnitudes, as they strongly depend on the exact geometry of the detector and on the gas filling it. The figure should only be taken as a general illustration of the expected behavior of a cylindrical counter.

At low applied voltages, this detector operates just like a cylindrical ionization chamber (the relative region is marked as "Ionization chamber" in the figure). However, at sufficiently large voltages, a sharp rise of the current is seen – an indication of the beginning of electron avalanche multiplication.

1.3 Avalanche and Discharge Development in Uniform or Cylindrical Electric Fields

Electron avalanche multiplication in gases was first observed, and then carefully studied, by John Sealy Townsend between 1897 and 1901. This process starts at some critical value of E/n_A (E being the electric field strength and n_A the gas number density, that is, the number of molecules or atoms per cubic meter), which depends on the geometry of the gas-filled space in which this phenomenon takes place. A free electron, drifting in the gas under the influence of the electric field, experiences various types of collisions with the atoms and molecules surrounding it, which can roughly be classified into two categories: elastic and inelastic. During elastic collisions, the electron only changes the direction of its motion,

but it does not lose its kinetic energy. As a result, the electron, after traversing a zone characterized by a potential difference of ΔV, will gain a kinetic energy:

$$E_{\mathrm{k}} = |q_e|\Delta V, \tag{1.3}$$

where q_{e} is the elementary electric charge of the electron.

Inelastic collisions are relevant at elevated electric fields; the electron loses part of its kinetic energy, and this leads either to the excitation of various levels of atoms or molecules (electronic for atoms, rotational, vibrational, and electronic for molecules) or to their ionization. In the latter case, another free electron, additional to the previous, appears in the gas volume (see Figure 1.5).

In the simplest case of electric field E with parallel field lines directed along the x axis, the infinitesimal increase $\mathrm{d}n_{\mathrm{e}}$ of the number of free electrons n_{e} in an avalanche process can be described mathematically as

$$\mathrm{d}n_{\mathrm{e}} = \alpha n_{\mathrm{e}} \mathrm{d}x \tag{1.4}$$

where α is the so-called first Townsend coefficient, expressing the probability for an electron to generate additional ion-electron pairs per unit length, which depends on E; note that gaseous detector usually operate at constant pressure, so here we neglect the dependance on n_A. By integrating Equation (1.4), one obtains that

$$n_{\mathrm{e}} = \exp(\alpha d), \tag{1.5}$$

with d being the distance across which the avalanche develops (eventually limited mechanically by the electrodes, which define the gap width in the case of a detector with parallel plate geometry).

If n_0 primary electrons located at $x = 0$ initiate an avalanche, then the total number n_{e} of created electrons will be proportional to n_0 (every time in a detector, the output signal is proportional to the total number of primary electrons the term

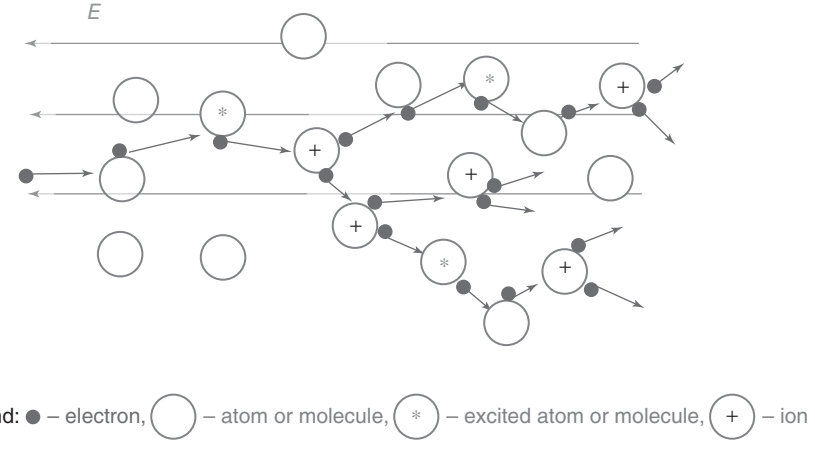

Figure 1.5 Schematics of the Townsend avalanche development in a gas: a free electron (coming from the left) drifting in an electric field intense enough experiences elastic and inelastic collisions with atoms and molecules, resulting in the creation of new free electrons, plus excited or ionized atomic or molecular species.

"proportional counter" is generally used):

$$n_e = n_0 \exp(\alpha d) \tag{1.6}$$

and the value

$$A = \exp(\alpha d) \tag{1.7}$$

is often called the multiplication factor or "gas gain," or simply "gain."

In the case of a nonuniform electric field in the gas, the gain has a more complicated form:

$$A = \exp\left(\int_a^b \alpha\{E(x)\}\mathrm{d}x\right) \tag{1.8}$$

which only in simple cases can be computed analytically and in most cases must be calculated numerically; in this case, a and b represent the coordinates of the initial and final point of the avalanche. For instance, for a single-wire counter, like the one described in Figure 1.3a;

$$A = \exp\left(\int_{r_a}^{r_c} \alpha(r)\mathrm{d}r\right), \tag{1.9}$$

where r_a and r_c are the radius of the anode and the cathode, respectively.

Note that electron drift velocity $v\_(E)$ in an electric field is much larger than the the ion drift velocity v_+, typically by a factor on the order of 1000. As a result, the avalanche consists of two parts: a fast "head" moving toward the anode, created by energetic electrons, and, remaining behind, a conical-shape "body" consisting in positive ions slowly drifting in the opposite direction.

The avalanche structure in the case of the parallel-plate geometry is shown in Figure 1.6 for two essential moments:

1) $t\_ = d/v\_$, when the avalanche electrons reach the anode;
2) $t_+ = d/v_+$, when the last positive ions reach the cathode.

For resistive plate chambers (RPCs), which is an important subject of this book described in detail in Chapter 3, the electric fields used are on the order of 50–100 kV/cm, and therefore typical values for $t\_$ are a few nanoseconds and for t_+ a few microseconds.

De-excitation of excited levels of atoms and molecules occurs via various channels. One of the most important among them in practice is ultraviolet (UV) photon emission which, due to the high energy of photons, can cause photoionization of the surrounding atoms and molecules, so that some secondary additional free electrons – called photoelectrons – can be created inside and outside the avalanche volumes (e.g., see Fonte *et al.*, 1991a), as also shown schematically in Figure 1.6a. This is sometimes also called an electron–photon feedback process.

One can introduce an overall probability γ_{ph} per avalanche electron to produce a new photoelectron. The total number n_{pe} of such secondary photoelectrons produced in an avalanche will be then:

$$n_{pe} = An_0\gamma_{ph}. \tag{1.10}$$

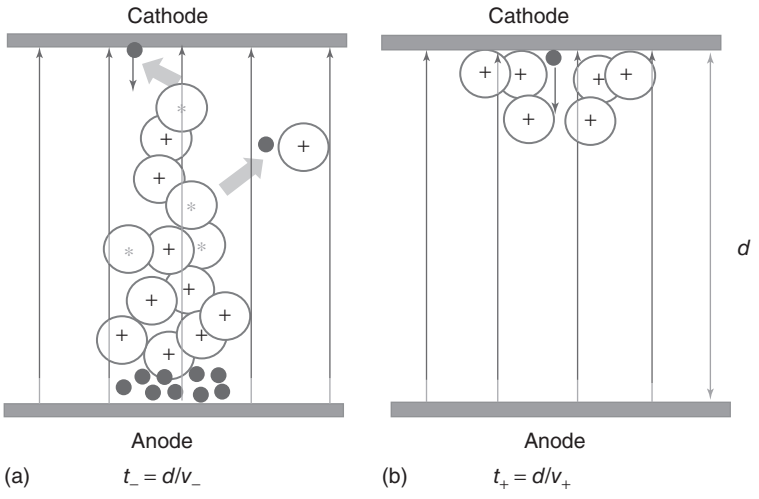

Figure 1.6 Schematic representation of the avalanche structure at two time intervals (a) $t_- = d/v_-$ showing also an electron created by gas self-photoionization; (b) $t_+ = d/v_+$, showing also a possible ion-ejected electron; $t = 0$ corresponds to the time when the avalanche was started by a single electron at the cathode. Small filled circles are electrons, open circles with a "+" sign in the center represent positive ions.

Note that the de-excitation of excited electronic levels leading to UV emission usually occurs quite rapidly, in a time much shorter than t_-.

The photoelectrons, being in a region where the electric field is not zero, may give rise to secondary avalanches as well; let us consider, in particular, the case when all photoelectrons are multiplied by the same gain A earlier defined. This happens in cylindrical wire counters when photoelectrons are created wherever in the gas volume or at the cathode, and in parallel plate chambers when all photoelectrons are created from – or very close – to the cathode. Even in this extreme case, if $A\gamma_{\text{ph}} \ll 1$ the photoelectron production process can be neglected, and the avalanche will be well localized in space (as it is represented in Figure 1.6a).

After the collection of all the avalanche electrons on the detector anode (which takes place around time t_-), ions still continue their slow drift and later on at some moment t_+ the last ones will reach the cathode (see Figure 1.6b).

As an ion approaches the cathode surface, it can be neutralized via electron tunneling from the cathode taking one of the electrons inside the conduction band of the material (Mc Daniel, 1964). Indicating with E_{i} the ion first ionization energy, and with φ the work function of the cathode (i.e., the energy needed to extract an electron from it), if $E_{\text{i}} > \varphi$ an excess in energy $E_{\text{ex}} = E_{\text{i}} - \varphi$ will result (see Figure 1.7). This can be transferred to another electron inside the cathode and, in the case of $E_{\text{ex}} > \varphi$ the electron can escape from it.

Overall, if the condition

$$E_{\text{i}} > 2\varphi \tag{1.11}$$

is met, a free electron can be emitted from the cathode as a result of ion recombination; the relative probability is indicated with γ_+ and it is sometimes called

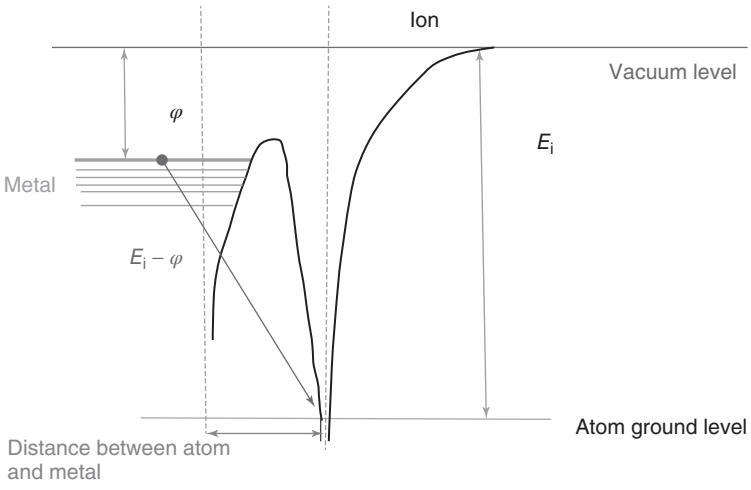

Figure 1.7 Schematic representation of the energy levels and tunneling effect of an ion approaching the metal electrode.

"second Townsend coefficient" (Davies and Evans, 1973). This electron emission initiates ion feedback.

In single-wire counters, when both $A\gamma_{ph}$ and $A\gamma_{+}$ are much less than unity, the amplitude S_d of the signals from the detector will be proportional to the primary ionization:

$$S_d = kAn_0, \tag{1.12}$$

where k is a proportionality coefficient depending on the actual induction process and electronics characteristics. The voltage interval where this behavior holds (between the "ionization chamber" region and the knee in "avalanche multiplication") is called the proportional region (see Figure 1.4).

In parallel plate chambers, as will be seen in detail in Chapter 3, even if this conditions is met, there is often no proportionality between the primary ionization and the output signal, since in this case the gain A depends strongly on the position inside the gas volume where the ion-electron pairs are created. For other detectors, like mesh detectors (for instance MICROMEGAS) which is described later on in this book, Equation (1.12) is still valid, provided that the drift volume and the amplification volume are separated.

The development of avalanches depends on their size. When this is sufficiently small, it can be safely assumed that the local electric field is almost entirely due to the external electric field (which, for instance, depends on electrode configuration, and applied voltage). However, it must be noted that the electric field inside an avalanche, generated by the spatial separation between the "head," negatively charged, and the "body" of the avalanche, positively charged, is opposite in direction with respect to the external field. For sufficiently large avalanches, this "space charge field" – as it is usually called – cannot be neglected anymore, and affects avalanche development. The appearance of space-charge effects is signaled in Figure 1.4 by the fact that the gas gain curve begins deviating from the

straight line (in a logarithmic scale). In single-wire counters, this is usually taken as the end of the proportional region.

Space-charge effects, briefly mentioned here, play a very important role in the operation of some resistive detectors; in particular, when a parallel-plate configuration with quite thin (order of a few hundred micrometers) gaps are used. This is discussed in detail later on, in particular in Chapter 4.

Increasing the applied voltage beyond the proportional region, in the interval labeled as "Geiger mode" in Figure 1.4, the amplitude of all pulses from the detector becomes almost equal to each other, independent of the primary ionization n_0.

Depending on the gas, in this region, or with another further gain increase, if either $A\gamma_{\text{ph}}$ or $A\gamma_{+}$ starts approaching unity, secondary processes strongly affect the detector operation: each primary electron is accompanied by one or even more secondary avalanches called "successors." Finally, at $A\gamma_{\text{ph}} = 1$ or $A\gamma_{+} = 1$ (whichever condition comes first), a continuous discharge appears (in the region marked in Figure 1.4 as "corona discharge").

Strictly speaking, Geiger mode is just an unstable corona discharge (Nappi and Peskov, 2013), so there is not a clear distinction between the two operation modes. In early designs, large resistors, 100 MΩ or larger, were always used in the electric circuits of single-wire counters, connected in series with the high-voltage power supply (as shown in Figure 1.3b). A corona current (which is typically a few microamperes) causes a significant voltage drop ΔV, of even a few hundred volts, on such resistors, consequently reducing the voltage across the detector and temporarily lowering the electric field in the gas; this, as a consequence, leads to the interruption of the corona discharge. In this counter, the output signal is taken measuring the voltage across the quenching resistor; therefore, a voltage drop ΔV of the magnitude mentioned would indicate the passage of an ionizing particle. At the beginning of the last century, when electronics was still at an initial stage of development, wire counters operating in Geiger mode offered the possibility of recording single charged particles or photons in a very simple way, without using amplifiers. This feature determined the tremendous success of the Geiger counters at that time.

It is interesting to note that although single-wire counters were not resistive detectors in the sense used in this book (where detectors in which resistive elements are embedded in their structure are mainly treated), they were the first in which the principle of discharge quenching with the help of resistive elements (the resistor put in series with the power supply) was implemented. As will be shown subsequently, the principle exploited in modern resistive detectors has many similarities with it.

Note also that later on it was discovered (Trost, 1937) that in some gas mixtures another mode of operation appears, in which the discharge is quenched not by the external resistor, but by intrinsic mechanisms, one of them being the strong space charge created by the corona discharge around the anode wire (see Nappi and Peskov, 2013 for more details).

Until the 1950s, Geiger and proportional counters were practically the only electronic detectors of elementary particles. When parallel-plate devices were also introduced, the details of avalanche development and feedback processes

were carefully studied in many gases and gas mixtures, both for cylindrical and parallel-plate geometry. Various methods were used, including the visualization of these phenomena with the help of Wilson cameras, which revealed many important peculiarities (see, for instance, Raether, 1964 and references therein).

It was observed that at low gas gains, the avalanche dynamic is quite similar for both cylindrical and parallel-plate geometries; however, at high gas gains, differences appear. In particular, in the case of the parallel-plate geometry, one of the two following modes of operation occurs (for more details, see Fonte *et al*., 1991b):

1) A "fast" breakdown or
2) A "slow" breakdown.

1.3.1 Fast Breakdown

In most of the cases, at some critical total charge in the avalanche, a transition from primary avalanches to sparks was observed. Scrupulous studies, performed by Raether (e.g., see Raether, 1964) showed that for parallel-plate detectors this happens when

$$An_0 \gtrsim 10^8 \text{ electrons} \tag{1.13}$$

In this condition, often called the "Raether limit," the electric field generated close to the "head" of the avalanche by the space charge becomes comparable with the external applied field. Consequently, the field lines in the vicinity of the avalanche are bent toward the positive "body" of the avalanche, made primarily of ions (see Figure 1.8a). Due to this focusing effect, with a consequent increase of the field strength in this region, secondary avalanches initiated close to the volume of the primary avalanche start drifting toward the "body" while they are strongly multiplicated because of the enhanced electric field nearby. The ionic column thus grows quite rapidly toward the cathode, leading to the formation of

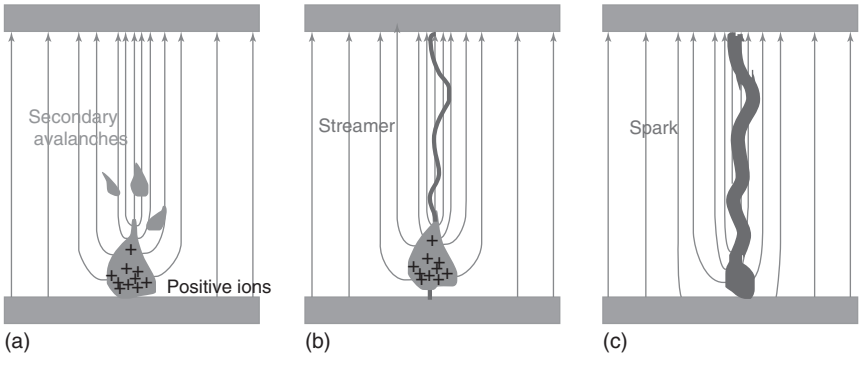

Figure 1.8 Three stages of spark development, when the total charge in the avalanche reaches the Raether limit: (a) field lines close to the avalanche experience a focusing effect and some secondary avalanches start moving toward the positive ions "body"; (b) a thin plasma filament – a streamer (or Kanal) – is formed; (c) when the streamer reaches the electrodes, a spark happens through the channel opened in this way.

a thin plasma channel, called streamer (or Kanal, or, sometimes, Kanal mechanism), schematically shown in Figure 1.8b. When the streamer touches the cathode, a powerful spark happens via this conductive channel (Figure 1.8c).

This process is called fast breakdown. Eventually, if no quenching mechanisms are in place, the spark will fully discharge the detector anode–cathode capacitance.

Note that if the voltage between the electrodes is further increased, the streamer may propagate not only to the cathode but to the anode as well; hence, the distinction of "cathode streamer" and "anode streamer."

It has been pointed out that photoelectrons produced via the mechanisms briefly outlined earlier in this chapter, play an important role in streamer development, and actually this is the common explanation for the streamer propagation mechanism (Raether, 1964). Nevertheless, this has been criticized (e.g., Kunhardt, 1980), on the grounds of whether the quantity and range of the relevant photons is adequate to sustain the streamer. Recent calculations (Capeillère *et al*., 2008) have further clarified that for the mechanism to be effective the photon range must lie within some boundaries, which is hardly a good explanatory basis for an almost universal phenomenon in gases. A possible, more robust, explanation is that diffusion – a truly universal phenomenon – may be enough to populate the high-gain regions of the streamer (Ebert *et al*., 1997). Vacuum ultraviolet (VUV in the following) and visible photons reaching the cathode can also create electrons via the photoelectric effect.

When the electric field is not uniform, in particular in the case of thick central wire detectors, where the field lines are radial in shape, an interesting phenomenon may happen. In this case, the streamer appears in the strong electric field close to the anode, and starts moving toward the cathode. However, when reaching a region of weak electric field far from the central wire, where multiplication processes are not so effective, it may suddenly stop propagating and decays without reaching the cathode (see Figure 1.9). This creates a fast, large-amplitude pulse current in the output readout circuit, but not a spark discharge (since there is no a conductive bridge between the cathode and the anode). This phenomenon is called "limited streamer mode" and this type of streamer is often called a "self-quenched streamer" (SQS). It typically appears

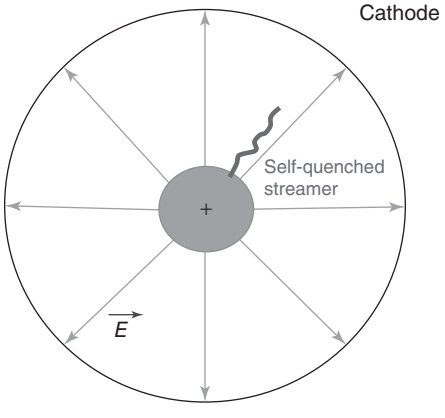

Figure 1.9 Schematic representation of a self-quenched streamer appearing in wire detectors having a certain ratio r_a/r_c.

in wire-type detectors characterized by a large ratio r_a/r_c. More details could be found in (Razin, 2001).

1.3.2 Slow Breakdown

Another type of breakdown, often called a "slow breakdown" (called so because it develops in a timescale of microseconds or even longer), also seldom appears in parallel-plate detectors, for example, when filled with very clean noble gases or when they are constructed with photocathodes having a high UV and visible photon sensitivity. In these cases, both γ_{ph} and γ_+ have exceptionally high values; therefore, the conditions $A\gamma_{ph} = 1$ or $A\gamma_+ = 1$ may be satisfied before the condition (1.13) $An_0 \gtrsim 10^8$. The slow breakdown develops via the generation of several or, sometimes, even up to dozens, secondary processes (Raether, 1964). Similarly to Geiger discharges, the region where the secondary avalanches appear rapidly expands in space; however, the final stage of this development strongly depends on the gas composition, pressure, and the detector geometry. In most of the cases, it also leads to a spark, however in some occasions could also be considered a kind of glow discharge.

1.4 Pulsed Spark and Streamer Detectors

There were early attempts to record radiation, also at the single particle level, with parallel-plate counters (e.g., see Keuffel, 1948); however, when using a constant applied voltage, their behavior was sometimes very unstable.

There were three main reasons for that:

1) If for some reason (e.g., due to the appearance of alpha particles, neutrons, or a cosmic shower) a large number of primary electrons was released in their volume, then the condition (1.13) $An_0 \gtrsim 10^8$ is verified, causing a spark breakdown.
2) Another problem was "after-pulses": a series of pulses following the primary avalanche, sometimes continuing for a long period of time.
3) Moreover, undesirable sparks often appeared due to the imperfection of electrode manufacturing: not well-rounded edges, micro-points or microinsertions (dust, etc) on the electrode surfaces.

A much more stable operation was achieved not using a constant applied high voltage, but using a pulsed (or triggered) mode of operation.

In this case, a relatively "low" constant voltage (on the order of a few kilovolts) was applied continuously to a parallel-plate detector, surrounded either by a scintillator-based triggering device (see Figure 1.10) or by an array of Geiger counters. When a charged particle crossed the scintillators (or Geiger counters) and, consequently the parallel-plate detector therein, a trigger signal was generated by the scintillators (or Geiger counters).

Using some kind of electronics, at this moment a short (on the order of microseconds) high-voltage pulse with an amplitude typically above HV = 10 kV (the exact value depending on the particular design and gas composition) was

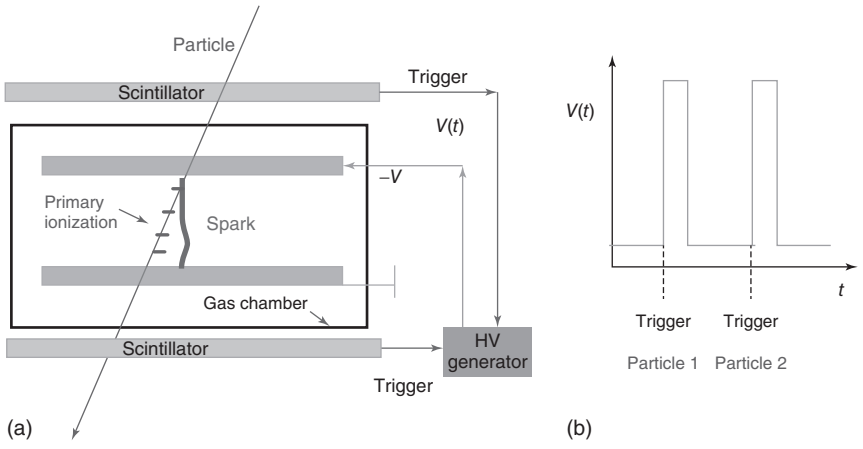

Figure 1.10 Simplified drawing of a spark counter, surrounded by scintillators and operating in a pulse mode.

applied to the electrodes of the parallel-plate detector. In this high electric field, the primary electrons created by the passing particle (and already kept apart from ions due to the low constant electric field) initiate Townsend avalanches which then rapidly transit to a spark. The position of the spark was recorded by photographic methods. To visualize the particle track, a stack of such parallel-plate detectors was used.

The low voltage between the pulsed HV was necessary to "clean up" the gap from undesirable ions appearing there for any reason: electron emission from electrodes, cosmic rays, natural radioactivity, residual ions from the previous sparks, and so on.

Until the 1970s, spark counters were one of the main detectors of charged particles, which allowed visualizing particle trajectories, and they successfully competed with emulsion films and cloud and bubble chambers.

In particular, the advantage of spark counters with respect to its competitors was their unprecedented fast response time (on the order of nanoseconds), which was quite important in high-energy and astrophysics experiments. However, due to their peculiar operation mode, spark counters had also serious drawbacks: relatively low operational rates, limited by the dead time (inactive in between HV pulses), which is typically about 0.01 s (e.g., see Gajon and Lksin, 1963); long readout time, on the order of milliseconds, imposed by the photographic or film readout techniques, so the data was only available offline; problems in recording several events happening at the same time; rather complicated designs.

A remarkable modification of the spark counter was the so-called streamer chamber. In these detectors, the duration of the HV pulse was only a few nanoseconds – which was remarkable at the time – and the (single) gap was relatively wide, on the order of centimeters. During this extremely short time interval, streamers started developing near the primary electrons created by the particle but remained too small in length to trigger sparks, producing at the same time sufficient light to make visible in three dimensions (3D) the trajectories of

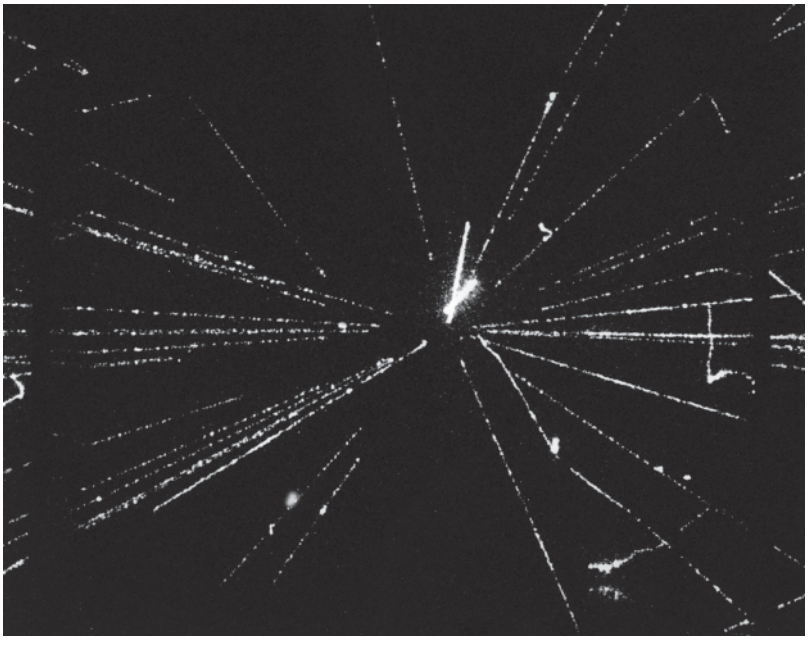

Figure 1.11 A proton–antiproton collision recorded using a streamer chamber at the UA5 experiment at CERN. (https://commons.wikimedia.org/wiki/File:CERN_UA5_-_ppbar_interaction_at_540GeV.jpg. Licenced under CC BY 3.0.)

the particles impinging on the device. A nice picture obtained with a streamer chamber is shown in Figure 1.11. Although these devices were able to detect multiple tracks, they remained too slow, due to the long "dead" time between pulses and the photographic readout technique used.

1.5 Multiwire Proportional Chambers

In 1968 G. Charpak invented a new avalanche gaseous detector, which he called the multiwire proportional chamber (MWPC) (Charpak *et al*., 1968). In contrast to spark and streamer chambers, it was a continuously operating device, thus self-triggering, with a fast electronic readout allowing to record events even at a high rate (even up to 10^5 Hz/wire), including multiple tracks. This detector is represented schematically in Figure 1.12a,b.

The first version of the MWPC (see Figure 1.12a) consisted of two parallel cathode planes with an array of thin parallel anode wires stretched in between, usually in the middle. Typically, the anode pitch, depending on the particular design, was in the 3–6 mm range, while the anode–cathode gap was around 5–8 mm. The charged particles crossing the MWPC would produce primary electrons in the gas volume, which will drift toward the anode wires. As they approach the anode at a distance typically around a few anode radius, where the electric field is more intense, the primary electrons give rise to Townsend avalanches developing close to the wires. The avalanches induce negative electronic signals on

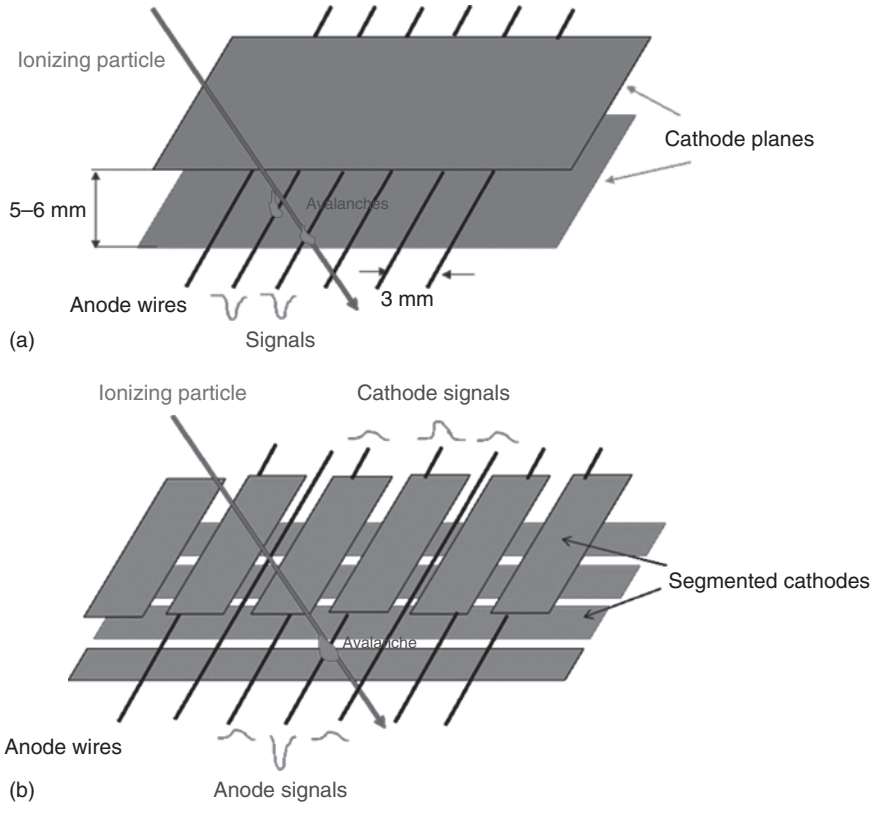

Figure 1.12 Schematics of a MWPC: (a) the first version of an MWPC with unsegmented cathode plane and (b) modern design of a bi-dimensionally sensitive MWPC, with cathodes segmented for isolation from each other's parts (strips, wires, etc.).

the anodic wires, where electrons are collected, and positive signals on the surrounding electrodes. Overall, this process is very similar to the one happening in single-wire counters, and in fact an MWPC can be considered as an array of single-wire counters, which share the gas volume and the cathode electrodes.

Originally, this detector could provide the coordinates of an impinging particle in one direction only: in fact, the signals were read out from the anode wires and one could just measure which wire was interested by the avalanche process. As a consequence, only the position of the avalanche in the direction perpendicular to the wires (and parallel to the cathodes) could be measured.

Later on, the signals induced on the other electrodes also started to be exploited, allowing to determine the position of the avalanches in two dimensions. One way of implementing this approach was to use cathodes segmented in strips, as shown in Figure 1.12b, and connecting each cathodic strip to its own readout circuit. Positive avalanche ions drifting toward the cathode induce signals on the closest strips and from the profile of the induced charges one can determine the avalanche position with an accuracy of about a few hundreds

micrometers (down to 14 μm in special cases Fischer *et al*., 1986), which is comparable to the earlier spark and streamer detectors.

Another advantage of MWPCs is that, in contrast to the spark and streamer chambers, they operate in proportional mode, and the output signal is proportional to the primary ionization n_0. Sparks rarely happen in well-designed MWPCs, but they may arise mainly due to construction defects such as sharp metallic edges, unprotected wire tips, dielectric insertions on the cathode or anodic wires, and so on. Various technical solutions were devised to protect the front-end electronics in the case of occasional sparks. For example, in the *R*ing *I*maging *CH*erenkov (RICH) detector of the ALICE (a large ion collider experiment) experiment at CERN (ALICE Collaboration, 2000), all anodic wires are connected to the HV supply via 10–100 MΩ resistors, whereas the signals are taken from the segmented cathode plane. In the event of undesirable sparks, the resistors will limit the discharge current just like it was done in the first Geiger counters (Figure 1.3).

In some particular gas mixtures and depending on particular conditions, it is possible to operate MWPCs in the Geiger or SQS modes (see, for example Peskov, 1979), and this has found some practical use (Bałanda *et al*., 2004).

Thanks to their excellent characteristics, MWPCs and their descendants (drift chambers, time projection chambers, etc.) rapidly replaced spark and streamer counters, as well as cloud and bubble chambers, in most high-energy physics experiments. Moreover, MWPCs filled with photosensitive vapors (Seguinot and Ypsilantis, 1977; Bogomolov *et al*., 1978) played a very important role in the development of RICH detectors (Seguinot and Ypsilantis, 1994). However, despite their tremendous success, MWPCs suffered from an essential drawback: a limited time resolution, on the order of microseconds. This derives from the fact that primary electrons can be released essentially anywhere in the detector volume and have to drift to the nearest anode wire, producing an avalanche there. The drift time is quite variable and the time jitter is almost equal to the maximum drift time.

1.6 A New Idea for Discharge Quenching and Localization

As the technology in particle physics detectors progressed, new high energy physics experiments demanded not only high spatial resolution and fast electronic readout but also better timing characteristics. An interest in parallel-plate geometry detectors, offering a minimal jitter and thus excellent timing, appeared again after the invention of the so-called continuous operation spark counters (Babykin *et al*., 1956; Parkhomchuk *et al*., 1971). A very practical and successful implementation of these concepts, later on, brought about the birth of the RPCs in the 1980s (Santonico and Cardarelli, 1981).

A simplified drawing of this innovative device, which is described in more detail in Chapter 3, is shown in Figure 1.13. At a first glance it resembles very much a spark counter, but with a fundamental difference: its electrodes are not made

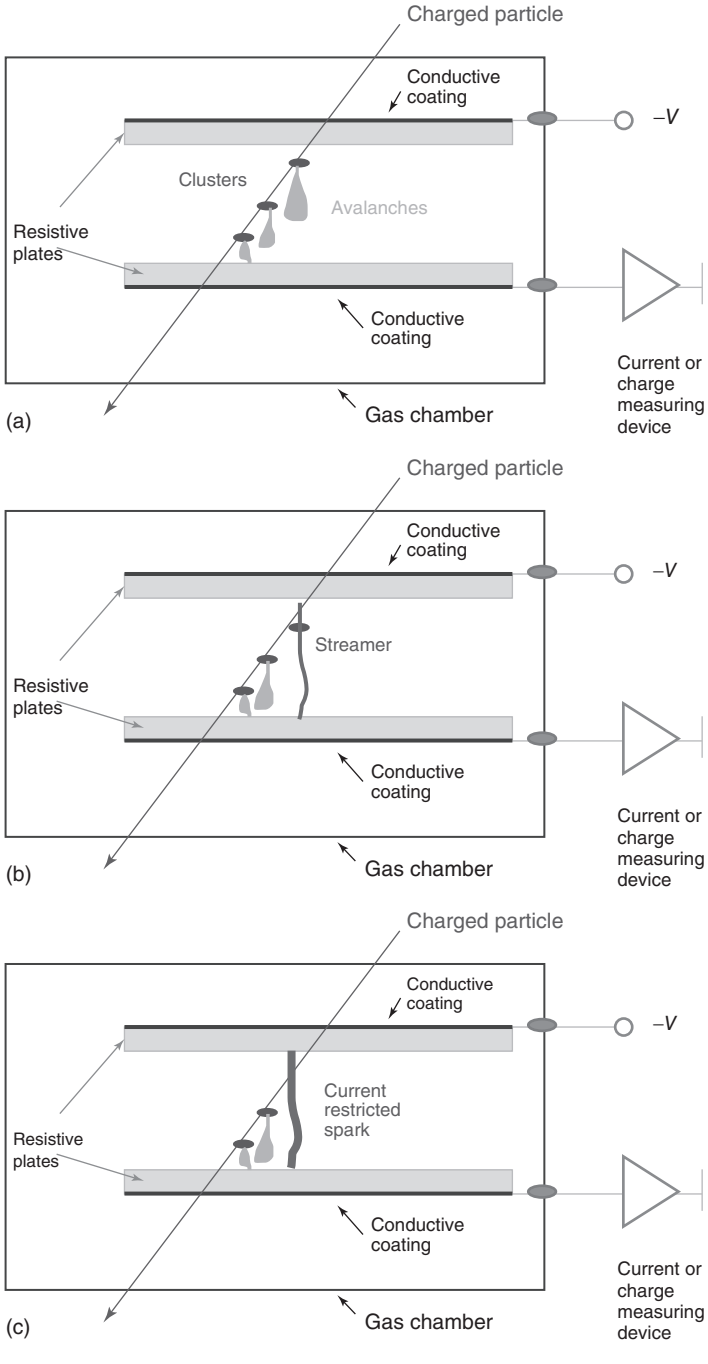

Figure 1.13 Schematic drawing of an RPC illustrating its design and operation principle: (a) creation of avalanches by primary electrons produced by ionizing charged particles crossing the detector; (b) if the total charge in the avalanche reaches the Raether limit, the avalanche transforms to a streamer; (c) when the streamer reaches the resistive electrodes, it causes a local discharge; nevertheless, the released energy in the spark is strongly limited by the resistance of the plates.

of metal, but of materials with a relatively high electrical resistivity, typically in the 10^{10}–10^{12} Ω cm range, made with 1–2 mm Bakelite or glass plates. The outer surfaces of these electrodes are coated with a conductive or semiconductive layer to allow a reliable connection with an external applied constant high voltage.

In the gap between the plates, filled with a suitable gas, a uniform electric field is generated by the HV connected to the electrode plates and, if the field is strong enough, the primary electrons produced by impinging ionizing particles give rise to Townsend avalanches. The first stage of avalanche development, before reaching the electrodes, is quite the same as in classical spark counters, and if the total charge in the avalanche approaches or overcomes the Rather limit, the avalanche transforms to a streamer. However, when the streamer touches the resistive electrodes, a quite new phenomenon takes place.

In contrast to metals, the resistive cathode plate is unable to feed the streamer with a high current density since, generally, high resistivity materials are not efficient electron emitters. Moreover, the anode plate is not an ideal dielectric, but rather a high resistivity layer, which, under the applied high voltage, becomes positively charged. Therefore , when an avalanche or a streamer reaches the anode surface, this gets locally discharged (see Figure 1.14). This causes a local reduction in the electric field intensity, drastically reducing the charge supporting processes.

Both phenomena contribute to the restriction of the discharge current, even if most probably the local partial discharging effect is dominant. This was clearly demonstrated with an RPC, whose cathode was metallic and whose anode resistive: the power dissipated in the discharge in this case was almost the same as in an RPC having both electrodes made of resistive material (T. Francke, private communication).

The role of the partial discharging effect, and the role of the resistive electrodes, can be better understood from Figure 1.15, which shows a simplified circuit model of an RPC. From a semi-quantitative point of view, an RPC has

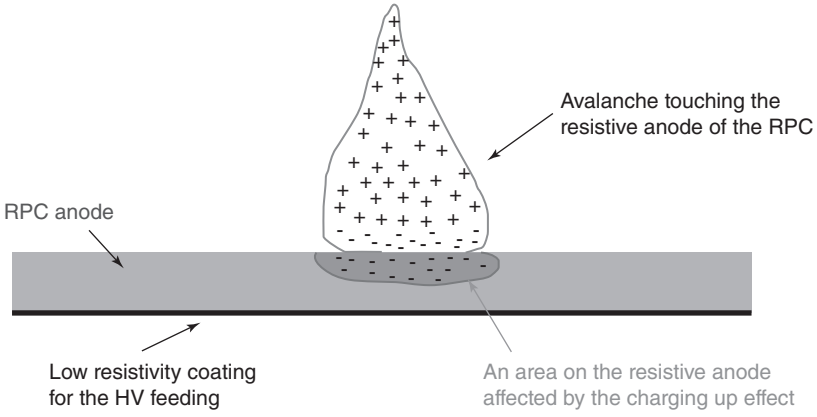

Figure 1.14 Schematic representation of the avalanche and the local partial anode discharging at the moment when the avalanche touches the dielectric anode.

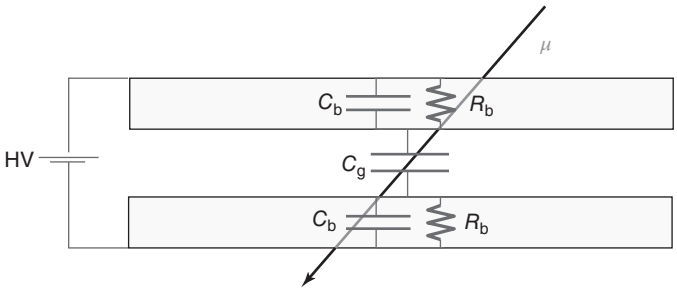

Figure 1.15 Simplified circuit for an RPC with resistive electrodes. C_b and C_g represent the capacitance of each electrode plate and of the gas gap, respectively; R_b represents the resistance of the electrode plates.

the structure of a capacitor, with two layers of dielectric material at its interior; moreover, the electrodes are made by resistive material, and this fact is taken into account considering their resistance R_b as shown in Figure 1.15. Basically, two situations can happen:

1) The gas is not ionized. In this "static" situation, the applied voltage HV is correspondingly transferred to the gas gap, and no current is flowing through the circuit.
2) The gas is crossed by an ionizing particle. In this case, the related discharge can be modeled as a current generator, which discharges the capacitor C_g (associated to the gas gap) in such a way that the voltage initially applied to the gas is transferred to the resistive electrodes (described by the capacity C_b and, as already pointed out, by the resistance R_b). The system comes back to the initial configuration following an exponential law, with a characteristic time constant τ given by

$$\tau = 2R_b\left(\frac{C_b}{2} + C_g\right) = 2\rho_b\frac{d}{S}\left(\frac{1}{2}\varepsilon_0\varepsilon_r\frac{S}{d} + \varepsilon_0\frac{S}{g}\right) = \rho_b\varepsilon_0\left(\varepsilon_r + 2\frac{d}{g}\right) \tag{1.14}$$

where ε_r is the relative dielectric constant of the electrode material, ρ_b its resistivity, ε_0 is the dielectric constant of the vacuum, g is the gas gap thickness, d is the thickness of the electrodes, and S is the electrode surface considered. Note that τ does not depend on the dimension S of the zone considered on the electrode. The spark quenching effect is stronger when C_b is small, so the thickness of the anode plate and its dielectric constant play an important role.

Equation (1.14) gives, for a value $\rho_b = 10^{11}\ \Omega\,\text{cm}$, a time constant τ around 10 ms, which has to be compared to the typical avalanche or discharge durations which are on the order of 10 ns $\ll \tau$. In this time interval, the electrodes behave as perfect dielectric materials; in other words, they are perfect insulators, and therefore the voltage across the gas gap is very low and the discharge inside the gas cannot be sustained. This is the auto quenching mechanism at the base of the operation of this detector. For the typical resistivities used in RPCs (see preceding text), the discharge current is reduced by orders of magnitudes when compared to spark counters with metallic electrodes.

In contrast to classical spark counters, where after the discharge the voltage drops in the entire gap, RPCs remain sensitive to incoming particles on the whole area unaffected by the local partial discharge effect (and the sensitivity drops only in the region of the given avalanche/streamer). This is why in early days this detector was often referred to as a continuously operating spark counter. After a time span a few times τ, the voltage on this small area is restored and the detector becomes again efficient in this area. Of course, the presence of resistive materials imposes some counting rate limitation owing to voltage drops across these.

In this simplified model of the RPC operation, the current leaks along the electrode surfaces as well as the influence of spacers, used to keep the electrode parallel, were not taken into account. These effects are considered later on in this book.

Summarizing, the unique features of RPCs are as follows:

1) It is a continuously operating detector (no need of pulsed HV for discharge quenching).
2) It has imaging capability, thanks also to its good spatial resolution (in some state-of-the-art designs 30–50 μm).
3) It has multi-hit capability, meaning that it can detect many events, even simultaneously.
4) It has a superior time resolution (in the most sophisticated configurations often below 50 ps);
5) Discharges in RPCs have limited energy and thus are not harmful – they do not destroy either the detector or the front-end electronics;
6) The size of the region affected by the charging up effect is relatively small, so the rest of the chamber remains active;
7) RPCs can be electronically read out, and this has many advantages compared to the optical recording, for example, in speed and image processing;
8) RPCs are relatively easy to build and they are suitable to cover large sensitive areas, in some experiments even up to thousands of square meters.

Later on in this book, we describe in more detail various RPC designs, the physics behind their operation, as well as the fast growing application of these devices.

References

ALICE Collaboration (2000) Time of Flight System. Technical Design Report, CERN/LHCC 2000-12, CERN, Geneva, Switzerland.

Babykin, M.V. *et al*. (1956) Plane-parallel spark counters for the measurement of small times; resolving time of spark counters. *Sov. J. At. Energy*, **4**, 627.

Bałanda, A. *et al*. (2004) The HADES pre-shower detector. *Nucl. Instrum. Methods Phys. Res., Sect. A*, **531**, 445–458.

Bogomolov, G. *et al*. (1978) Multiwire gas counters for coordinate measurements in the VUV region. *Instrum. Exp. Dent. Tech.*, **21**, 778–782.

Capeillère, J. *et al*. (2008) The finite volume method solution of the radiative transfer equation for photon transport in non-thermal gas discharges: application to the

calculation of photoionization in streamer discharges. *J. Phys. D: Appl. Phys.*, **41**, 234018, 13 pp.
Charpak, G. *et al*. (1968) The use of multiwire proportional counters to select and localize charged particles. *Nucl. Instrum. Methods*, **62**, 262.
Davies, A.J. and Evans, C.J. (1973) The Theory of Ionization Growth in Gases Under Pulsed and Static Conditions. CERN Yellow Report 73-10, CERN, Geneva, Switzerland.
Ebert, U., van Saarloos, W., and Caroli, C. (1997) Propagation and structure of planar streamer fronts. *Phys. Rev. E*, **55** (2), 1530–1549.
Fischer, J., Radeka, V., and Smith, G.C. (1986) X-ray position detection in the region of 6 μm RMS with wire proportional chambers. *Nucl. Instrum. Methods Phys. Res., Sect. A*, **252**, 239–245.
Fonte, P. *et al*. (1991a) VUV emission and breakdown in parallel-plate chambers. *Nucl. Instrum Methods Phys. Res., Sect. A*, **310**, 140–145.
Fonte, P. *et al*. (1991b) Feedback and breakdown in parallel-plate chambers. *Nucl. Instrum Methods Phys. Res., Sect. A*, **305**, 91–110.
Gajon, M.I. and Lksin, G.A. (1963) Spark detectors for charged particles. *Sov. Phys. Usp.*, **6**, 428.
Keuffel, J. (1948) Parallel-plate counters and the measurement of very small time intervals. *Phys. Rev.*, **73**, 531.
Khan, F.M. and Gibbon, J.P. (2014) *Khan's the Physics of Radiation Therapy*, Lippincott Williams & Wilkins/Wolters Kluwer.
Kunhardt, E.E. (1980) Electrical breakdown of gases: the prebreakdown stage. *IEEE Trans. Plasma Sci.*, **PS-8** (3), 130–138.
Mc Daniel, E.W. (1964) *Collision Phenomena in Ionized Gases*, John Wiley & Sons, Inc., New York.
Nappi, E. and Peskov, V. (2013) *Imaging Gaseous Detectors and their Applications*, Wiley-VCH Verlag GmbH & Co. KGaA.
Parkhomchuk, V.V. *et al*. (1971) A spark counter with large area. *Nucl. Instrum. Methods*, **93**, 269.
Peskov, V. (1979) Geiger counters of VUV and x-ray radiation with the spatial resolution of 0.3 mm. *Instruments and Experimental Techniques*, **22**, 1395–1400.
Raether, H. (1964) *Electron Avalanches and Breakdown in Gases*, Butterworths, London.
Razin, V.I. (2001) Self-quenched streamer operating mode of gas-discharge detectors (Review). *Instrum. Exp. Tech.*, **44** (4), 425–443.
Rutherford, E. and Geiger, H. (1908) An electrical method of counting the number of α particles from radioactive substances. *Proc. R. Soc. London, Ser. A*, **81** (546), 141–161.
Santonico, R. and Cardarelli, R. (1981) Development of resistive plate counters. *Nucl. Instrum. Methods Phys. Res.*, **187**, 377.
Seguinot, J. and Ypsilantis, T. (1977) Photo-ionization and Cherenkov ring imaging. *Nucl. Instrum. Methods*, **142**, 377–391.
Seguinot, J. and Ypsilantis, T. (1994) A historical survey of ring imaging counters. *Nucl. Instrum. Methods Phys. Res., Sect. A*, **343**, 1–29.
Trost, A. (1937) Über Zählrohre mit Dampfzusatz. *Z. Phys.*, **105**, 399.
Wikipedia, The Free Encyclopedia (2017) Ionization Chamber, https://en.wikipedia.org/wiki/Ionization_chamber (accessed 28 October 2017).